

Improving Super-Resolution Methods via Incremental Residual Learning

Muneeb Aadil Rafia Rahim Sibte ul Hussain
 Reveal Lab, National University of Computer and Emerging Sciences
 {il140140, rafia.rahim, sibteul.hussain}@nu.edu.pk

Abstract

Recently, deep Convolutional Neural Networks (CNNs) have shown promising performance in accurate reconstruction of high resolution (HR) image, given its low resolution (LR) counter-part. However, recent state-of-the-art methods operate primarily on LR image for memory efficiency, but we show that it comes at the cost of performance. Furthermore, because spatial dimensions of input and output of such networks do not match, its not possible to learn residuals in image space; we show that learning residuals in image space leads to performance enhancement. To this end, we propose a novel Incremental Residual Learning (IRL) framework to solve the above mentioned issues. In IRL, a set of branches i.e arbitrary image-to-image networks are trained sequentially where each branch takes spatially upsampled higher dimensional feature maps as input and predicts the residuals of all previous branches combined. We plug recent state of the art methods as base networks in IRL framework and demonstrate the consistent performance enhancement through extensive experiments on public benchmark datasets to set a new state of the art for super-resolution. Compared to the base networks our method incurs no extra memory overhead as only one branch is trained at a time. Furthermore, as our method is trained to learned residuals, complete set of branches are trained in only 20% of time relative to base network.

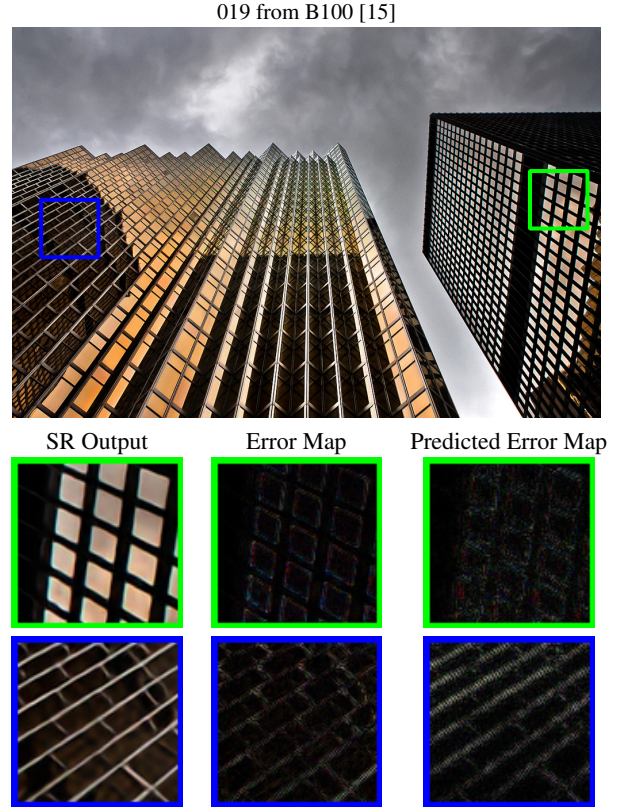


Figure 1: Prediction of error maps using our IRL framework. It successfully learns high frequency details.

1. Introduction

Single Image Super-Resolution (SR) aims to generate a High Resolution (HR) image I^{SR} from a low resolution (LR) image I^{LR} such that it is similar to original HR image I^{HR} . Formally speaking, the objective is to learn a mapping function $f(x)$ such that $I^{HR} \approx I^{SR}$ where $I^{SR} = f(I^{LR})$. SR has seen a lot of interest from the researchers recently because it is: (i) inherently an ill-posed inverse problem due to multiple possible outcomes; and (ii) an important low level computer vision problem having applications in many domains such as surveillance, or medical imaging etc.

With the success of Convolutional Neural Networks

(CNNs) for image transfer tasks, many researchers have recently applied CNNs based techniques for the problem of SR [3, 9, 10, 18, 19, 13, 14, 22, 12, 31] and have found it to be superior to older hand-crafted methods such as interpolation [30], reconstruction based methods [4, 27, 29] or dictionary based methods [26, 25, 20, 21]. Specifically, Dong *et al.* [3] (SRCNN) first introduced the idea of using CNNs for SR and showed significant improvement over prior methods. Their network takes an interpolated HR version of an image as input and applies 3 convolutional layers to refine the interpolated image. Kim *et al.* VDSR [9] tackled

training difficulties encountered in SRCNN [3] by explicitly modeling residuals in image space. This improvement not only made the training easier but it also made training of deep networks feasible. Following VDSR, later methods [10, 18, 19] focused on improving network architecture and showed enhanced performance. However, since these networks take an interpolated HR version of an image as input, they have high memory and computational requirements.

To tackle this issue, Ledig *et al.* [13] introduced SRResNet, it takes I^{LR} as input and apply convolutional operations primarily in LR space, followed by upsampling layers in the end to produce I^{SR} . This framework has become quite popular as almost all recent methods [14, 22, 12, 31] use upsampling layers in the end. Although these networks do not suffer from high memory requirements and expensive computational cost, they have two design limitations. Firstly, these networks upsample the feature maps too swiftly and thus are unable to reliably learn the content gap between LR space and HR space. Secondly, these networks cannot explicitly learn residuals in image space because spatial dimensions of input and output do not match.

We hypothesize that: (i) there is a large content-gap between the LR feature maps and desired HR output image and this gap cannot be reliably learnt in a single transition step using a convolutional layer; (ii) instead of directly modeling HR image, one should explicitly model residuals in image space to better model fine level details.

Thus, to this end, we propose the IRL framework: a new learning setup for SR task that improves the performance of existing networks. IRL uses an existing pre-trained network (called as master branch) and incrementally adds residual learning branches. Each added residual branch is the identical copy of the master branch, except it (i) is half as deep compared to master branch, (ii) works on upsampled feature maps, and (iii) is trained to learn the residuals of all previous branches combined. During training of each branch, all previous branches are kept freezed. At test time, the output of all branches are added to form the final output. On the computational front, improving a network using IRL only adds 20% extra training time and no extra memory overhead because of sequential training of the residuals. Our proposed architecture leads to consistent performance improvement of all the existing state-of-the-art SR networks.

Overall, we make following contributions: (i) a new learning strategy for smooth mapping from LR to HR images; (ii) a residual learning framework for learning the residuals in image space; and (iii) a new state-of-the-art for SR task.

2. Related Work

We decompose our discussion in two separate topics and review them separately in the following sections.

2.1. CNNs for Super Resolution

Recently, CNNs based methods have shown significant improvement for SR task and thus have proven strong potential for learning complex non-linear mapping from LR to HR space. Specifically, SRCNN [3] first introduced the idea of using CNNs for learning the SR task in end-to-end way and showed significant improvement over prior methods. VDSR [9] then tackled training difficulties encountered in SRCNN [3] by explicitly modeling residual learning in image space and proposed very deep 20 layers CNN inspired from VGGnet [17]. Similarly, DRCN [10] introduced parameters sharing in network using very deep recursive layers. Afterwards, DRRN [18] and MemNet [19] focused on improving network architectures. Specifically, DRRN [18] applied convolutional layers recursively to refine the image iteratively, and MemNet [19] employed memory block to take into account hierarchical information. However, since all these methods employ residual learning in image space, spatial dimensions of input image and target image must be same due to which these networks take as input an interpolated HR version of an image as input. Consequentially, these methods have high memory requirements and high computational cost.

To tackle this issue, recent approaches take input a LR image and apply convolutional operations primarily in LR space, followed by upsampling layers to produce an HR image. Since these methods apply majority of operations in the LR space, they do not suffer from high memory requirements and higher computational cost. For instance, SRResNet [13] adapts ResNet architecture [5] for SR and then employs ESPCNN [16] to upsample efficiently. Lim *et al.* [14] improves SRResNet [13] by removing unnecessary modules such as batch normalization and activation functions after upsampling and propose EDSR baseline (EDSRb) and EDSR which shows enhanced performance. SRDenseNet [22] employs DenseNet [6] architecture coupled with skip-connections to explicitly model low level features. LapSRN [12] employs laplacian pyramid style CNNs to iteratively upsample feature maps after processing feature maps on each scale and predicting residuals in image space. Then, very recently, RDN [31] merged residual block of EDSR [14] and dense skip connections of SRDenseNet [22] to form Residual Dense Block for improved low-level feature supervision which resulted in even better performance.

2.2. Objective Functions

Despite the fact that performance of neural networks are mainly driven by objective function, there hasn't been extensive studies investigating the role of loss functions in the context of SR except a few [8, 32, 13]. But typically, networks are either optimized on simpler pixel wise difference or more complex perceptually motivated objective functions. Because our work primarily focuses on optimiz-

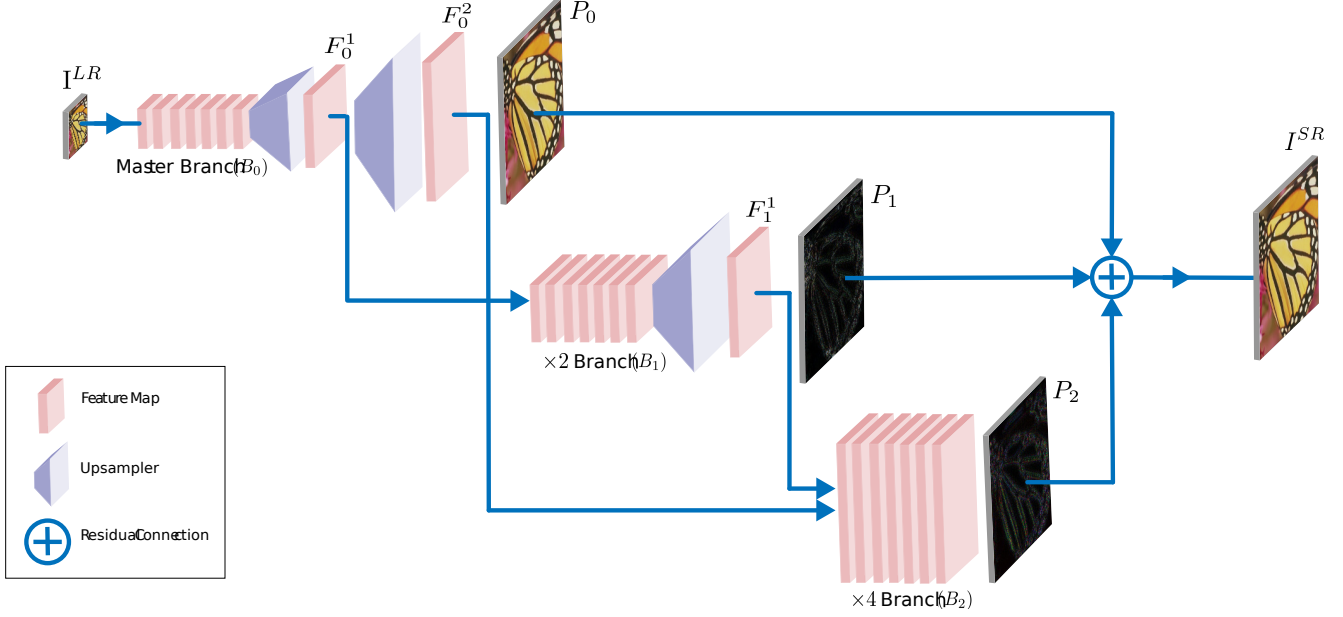


Figure 2: Our proposed IRL framework for $\times 4$ scale. Each branch represents an arbitrary image-to-image network. Its evolved from an existing architecture (master branch) by adding the residual branches ($\times 2$ and $\times 4$).

ing PSNR, perceptually motivated SR works are not discussed here.

Earlier networks majorly employ L_2 Loss because (i) it directly optimizes PSNR, and (ii) it has nice optimization properties [23]. However, Zhao *et al.* [32] has done extensive survey on effects of objective function on SR performance quantitatively and qualitatively. Specifically, it shows that L_1 loss outperforms L_2 in terms of PSNR. Qualitatively speaking, L_2 recovers high frequency information (edges) better than L_1 but it leaves splotchy artefacts on plain regions because it over-penalizes large errors and ignores small errors. On the other hand, L_1 loss removes splotchy artefacts at the cost of sharper edges recovery. Following [32], majority of the networks employ L_1 loss rather than L_2 loss.

3. Our Method

In this section, we describe our proposed framework and training methodology in detail. Firstly, a SR image-to-image network is selected as master branch and is trained typically on I^{HR} . When the training of master branch has converged, its weights are frozen and residual branch is added. This residual branch takes the upsampled feature maps of master branch and is trained on the residuals of master branch. This process is repeated until all scales of feature maps are processed – *c.f.* Figure 2.

We denote the set of branches with B_0, B_1, \dots, B_n where n are the number of branches. Number of branches

is dependent on SR scale. In our settings, we used 1 and 2 branches for $\times 2, \times 3$ and $\times 4$ scales, respectively. Each branch B_i produces a set of upsampled feature maps $F_i^1, F_i^2, \dots, F_i^{n-i}$, and a prediction P_i . Using this notation, we can formally state the methodology as follows:

$$P_i = \begin{cases} B_i(I^{LR}) & \text{if } i = 0 \\ B_i([F_0^i, F_1^{i-1}, \dots, F_{i-1}^1]) & \text{if } i > 0 \end{cases} \quad (1)$$

Where each branch B_i is trained on its respective label L_i which is formed as:

$$L_i = \begin{cases} I^{HR} & \text{if } i = 0 \\ R_i & \text{if } i > 0 \end{cases} \quad (2)$$

Where $R_i = I^{HR} - \sum_{k=0}^{i-1} P_k$. In the above equations, master branch and residual branches correspond to cases where $i = 0$ and $i > 0$, respectively.

Finally, at test time, result I^{SR} is formed as:

$$I^{SR} = \sum_{i=0}^n P_i \quad (3)$$

Although any arbitrary image-to-image SR network can be used as a master branch, we restrict our choices to recent state-of-the-art network to isolate the improvement caused by adding residual branches. We denote such networks by appending + or ++ to the original network's name depending on the number of residual branches added.

The following sections study in detail the effects of each component in our architecture.

3.1. Upsampled Feature Maps

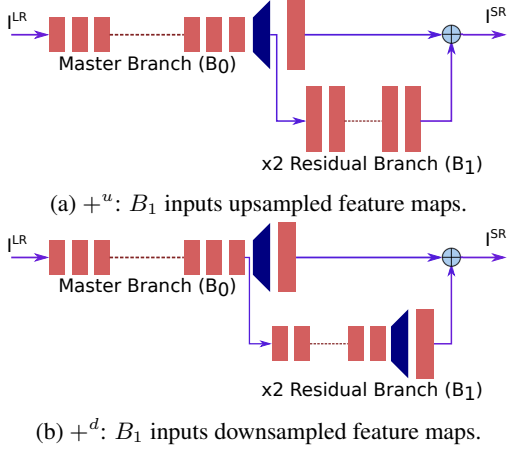


Figure 3: Comparison of our $+^u$ and $+^d$ variants.

In our setup, each branch operates on higher dimensional feature maps than previous branch. We argue that this design choice leads to performance enhancement. To confirm this, we isolated the difference caused by operating on upsampled feature maps and measured the performance enhancement. Specifically, we trained two variants: one takes as input the feature maps before upsampling layer in master branch (denoted as $+^d$), and one takes upsampled feature maps (denoted as $+^u$), as shown in figure 3. We then measured the performance difference between two variants. As shown in table 1, $+^u$ versions lead to enhanced performance consistently across all networks. Thus, for each branch, we used higher dimensional feature maps than previous branch. This way, we process multiple upscaled versions of feature maps. From now onwards, $+/+$ versions take upsampled feature maps, unless specified otherwise.

Network	Original	IRL (Ours)	
		$+^d$	$+^u$
LapSRN [12]	30.67	30.69	30.73
SRResNet [13]	29.80	29.81	29.84
EDSRb [14]	29.83	29.84	29.87
EDSR [14]	30.67	30.67	30.69
RDN [31]	30.64	30.65	30.67

Table 1: Comparison of performance in terms of PSNR (dB) of $+^d$ and $+^u$ versions on validation set for $\times 4$ scale.

Because spatial dimensions are doubled after every branch, each successive branch’s parameters have to be halved also to keep the memory requirements constant. Concisely, this requires us to either halving the number

of layers of the residual branches or the number of channels. We empirically found that our framework performs best when number of features are kept constant i.e when number of layers are halved. This finding is consistent with the findings of [14], *i.e.* feature maps are more important than the depth of the network – provided that the network is already deep enough.

3.2. Residual Learning in Image Space

Although residual branches can be trained to learn I^{HR} directly, we instead train them on image residuals because (i) it results in faster convergence [9], and (ii) it leads to slightly superior performance [9]. However, computing image residuals requires a candidate solution and HR image. Kim *et al.* [9] used bicubic interpolated image as a candidate solution and computed its residuals to be predicted by the network. However, since the master branch is already trained in our framework, we used the output of master branch as a reference to compute the residuals which are later predicted by residual branches.

3.3. Extending Contemporary State of the Arts

Network	Input	Original	IRL (Ours)	
			$+$	$++$
VDSR [9]	HR	30.58	30.58	30.58
DRRN [18]	HR	30.81	30.81	30.81
MemNet [19]	HR	30.86	30.86	30.86
LapSRN [12]	LR	30.67	30.73	30.76
SRResNet [13]	LR	29.80	29.84	29.87
EDSRb [14]	LR	29.83	29.87	29.89
EDSR [14]	LR	30.67	30.69	30.71
RDN [31]	LR	30.64	30.67	30.69

Table 2: Performance in terms of PSNR (dB) of $+$ and $++$ versions on validation set for $\times 4$ scale. Red and blue denotes the best and second best performance respectively.

To study the effect of adding IRL, we measured the performance improvement IRL causes – if at all – to existing state of the arts. Specifically, we used contemporary state-of-the-art networks in master branch and initialized from scratch networks residual branches, except the depth of network is halved after every subsequent branch because of the reason mentioned in previous section. For consistent experimentation, we keep training settings such as patch size, objective function the same as the one used for original state of the arts.

Table 2 summarizes the improvement of each network IRL causes for validation set. Our model consistently enhances the performance of each network taking LR input. However, IRL does not improve the performance at all for

the cases where network takes HR input. This is because the networks taking HR input already employ residual learning in image space and process upsampled feature maps.

3.4. Objective Functions

Zhao *et al.* [32] showed that L_1 loss outperforms L_2 in terms of PSNR. However, qualitatively speaking, L_2 loss recovers sharper edges while introducing splotchy artefacts in flat regions. While using L_1 loss significantly reduces splotchy artefacts introduced during training with L_2 loss, edges are not as sharp. Because all existing state of the arts explicitly model HR image without taking into account high and low frequency information separately, it can be trained with only one objective function at a time. Consequentially, a trade-off has to be selected between sharper edges and higher PSNR. However, because our framework has multiple branches, we can use different objective functions at the same time for different information to be learnt by each branch.

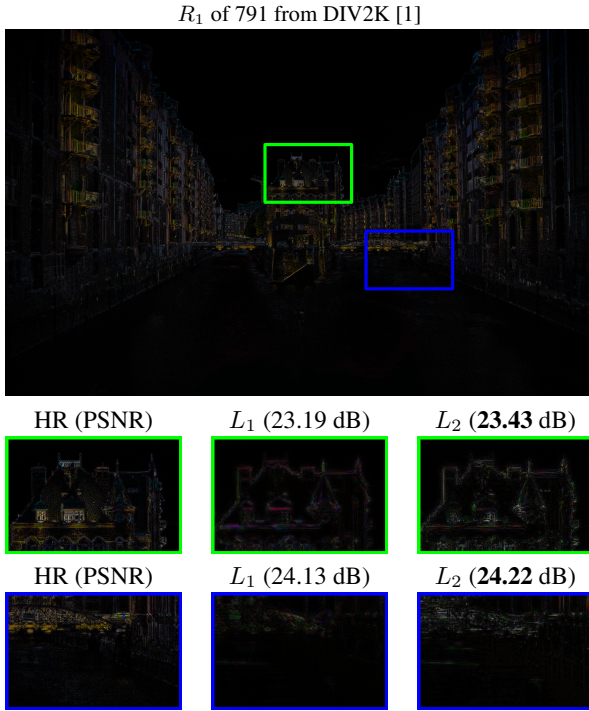


Figure 4: Comparison of L1 Loss and L2 Loss. L2 Loss performs better.

Specifically, different with the models trained in previous section, we trained the residual branches with L_2 loss instead of L_1 loss. Figure 4 shows the quantitative and qualitative comparison. L_2 loss not only recovers sharper edges, but it also performs better in terms of PSNR as opposed to previous works [14, 32]. We argue this is because previous works model HR image directly. On the other hand,

we explicitly model residuals i.e high frequency information. Because residuals are highly sparse, L_2 loss is suitable because of over-penalization of large errors while ignoring small errors.

4. Experiments

This section provides details on the dataset we have used, followed by implementation details for training. Finally, evaluation setup is explained along with quantitative and qualitative comparison with recent state-of-the-art methods.

4.1. Datasets

We trained our network on DIV2K dataset [1]: a newly proposed dataset by Timofte *et al.* for image restoration applications. It contains 800 training images, 100 validation images, and 100 test images. For training, we used first 790 images. For validation, we used remaining 10 images from DIV2K [1] training set – we explicitly have not used the provided validation set for validation. For evaluation, we used following publicly available benchmark datasets: Set5 [2], Set14 [28], B100 [15], and Urban100 [7].

4.2. Implementation Details

Learning rate was set to $1e^{-4}$ for all experiments. Each residual branch was trained for 30 epochs using ADAM [11] ($\beta_1 = 0.9, \beta_2 = 0.99$). Furthermore, we augment the training data with random horizontal flips and 90 rotations. LR image patch size during training was variable depending on the network used in master branch for consistent experimentation. Specific patch sizes for all networks used in master branch are mentioned in table 3.

Network	Patch Size
LapSRN [12]	32
SRResNet [13]	24
EDSRb [14]	24
EDSR [14]	24
RDN [31]	32

Table 3: LR image patch sizes used during training for different master branches

Since our work requires pre-trained weights of previous state of the arts, we downloaded the pre-trained weights of each network from their official implementations available online and imported them into our codebase. We developed IRL framework in Python using Pytorch framework and our code is publicly available online¹. All networks are trained on NVIDIA Tesla K80.

Scale	Method	Set5 [2]	Set14 [28]	B100 [15]	Urban100 [7]
$\times 2$	LapSRN [12]	37.52 / 0.9573	33.08 / 0.9121	31.80 / 0.8924	30.41 / 0.9091
	LapSRN+ (Ours)	37.55 / 0.9586	33.11 / 0.9122	31.82 / 0.8927	30.45 / 0.9093
	EDSRb [14]	37.98 / 0.9604	33.56 / 0.9173	32.15 / 0.8994	31.97 / 0.9271
	EDSRb+ (Ours)	38.01 / 0.9606	33.58 / 0.9174	32.18 / 0.8997	32.03 / 0.9276
	EDSR [14]	38.11 / 0.9602	33.92 / 0.9195	32.32 / 0.9013	32.93 / 0.9351
	EDSR+ (Ours)	38.14 / 0.9604	33.94 / 0.9196	32.34 / 0.9014	32.96 / 0.9354
	RDN [31]	38.23 / 0.9613	34.00 / 0.9211	32.33 / 0.9016	32.87 / 0.9352
	RDN+ (Ours)	38.27 / 0.9615	34.03 / 0.9214	32.36 / 0.9019	32.91 / 0.9355
$\times 3$	EDSRb [14]	34.36 / 0.9267	30.28 / 0.8415	29.08 / 0.8053	28.14 / 0.8525
	EDSRb+ (Ours)	34.41 / 0.9271	30.31 / 0.8417	29.11 / 0.8056	28.17 / 0.8528
	EDSR [14]	34.65 / 0.9282	30.52 / 0.8462	29.25 / 0.8093	28.80 / 0.8653
	EDSR+ (Ours)	34.68 / 0.9284	30.55 / 0.8465	29.28 / 0.8096	28.83 / 0.8655
	RDN [31]	34.70 / 0.9293	30.56 / 0.8467	29.25 / 0.8094	28.79 / 0.8651
	RDN+ (Ours)	34.73 / 0.9294	30.60 / 0.8469	29.27 / 0.8096	28.81 / 0.8654
$\times 4$	LapSRN [12]	31.62 / 0.8869	28.12 / 0.7718	27.33 / 0.7286	25.28 / 0.7602
	LapSRN+ (Ours)	31.64 / 0.8867	28.16 / 0.7716	27.35 / 0.7289	25.33 / 0.7608
	LapSRN++ (Ours)	31.67 / 0.8870	28.18 / 0.7718	27.37 / 0.7290	25.36 / 0.7612
	SRResNet [13]	32.05 / 0.8910	28.53 / 0.7804	27.57 / 0.7354	26.07 / 0.7839
	SRResNet+ (Ours)	32.08 / 0.8913	28.55 / 0.7807	27.59 / 0.7356	26.13 / 0.7844
	SRResNet++ (Ours)	32.10 / 0.8914	28.57 / 0.7808	27.62 / 0.7358	26.15 / 0.7845
	EDSRb [14]	32.09 / 0.8926	28.56 / 0.7808	27.56 / 0.7359	26.03 / 0.7846
	EDSRb+ (Ours)	32.13 / 0.8932	28.59 / 0.7816	27.59 / 0.7362	26.07 / 0.7848
	EDSRb++ (Ours)	32.15 / 0.8934	28.60 / 0.7817	27.60 / 0.7362	26.08 / 0.7849
	EDSR [14]	32.46 / 0.8968	28.80 / 0.7876	27.72 / 0.7420	26.64 / 0.8033
	EDSR+ (Ours)	32.48 / 0.8970	28.83 / 0.7878	27.75 / 0.7423	26.66 / 0.8034
	EDSR++ (Ours)	32.49 / 0.8971	28.84 / 0.7879	27.75 / 0.7424	26.69 / 0.8036
	RDN [31]	32.46 / 0.8980	28.80 / 0.7868	27.71 / 0.7420	26.61 / 0.8027
	RDN+ (Ours)	32.48 / 0.8982	28.82 / 0.7871	27.74 / 0.7424	26.63 / 0.8030
	RDN++ (Ours)	32.50 / 0.8982	28.84 / 0.7872	27.75 / 0.7424	26.64 / 0.8031

Table 4: Quantitative Results (PSNR (dB) / SSIM) of adding IRL framework to the existing state of the art methods on different benchmarks datasets. Our proposed framework leads to consistent performance improvement for all scales.

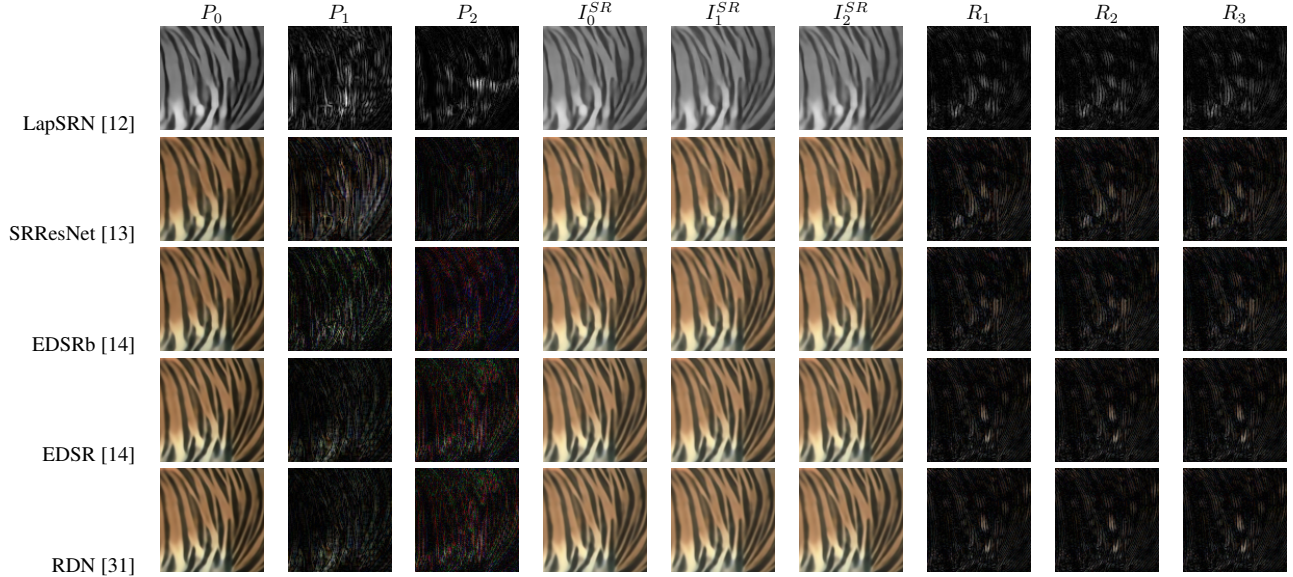
4.3. Benchmark Results

We apply and test our approach on the following state-of-the-art networks: LapSRN [12], SRResNet [13], EDSR baseline (EDSRb) [14], EDSR [14], RDN [31]. We skipped SRDenseNet [22] because neither there are any pre-trained weights, nor any publicly available implementation to train the network from scratch, unlike all mentioned networks we compared our approach with. Furthermore, we did not include methods taking interpolated HR image as input because they already process upsampled feature maps and learn residuals in image space. We measure PSNR and SSIM [24] values on only the Y-channel of transformed YCbCr image. For consistent comparison, we chop off the same amount of pixels as scale from the image borders. Table 4 shows quantitative results of adding one residual

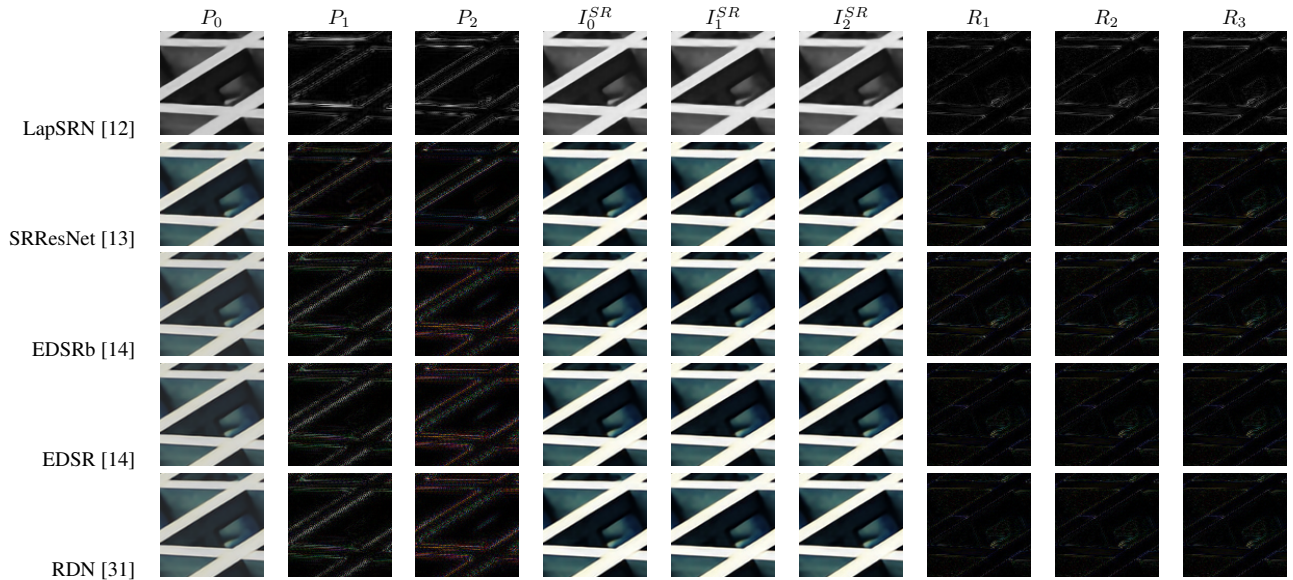
branch (+ versions) and two residual branches (++ versions) to the existing state of the arts on different benchmarks datasets for $\times 2$, $\times 3$, and $\times 4$ scale. Our proposed framework leads to consistent improvement in the performance of existing methods for all scales.

Figure 5 demonstrates the qualitative improvement IRL causes for each network. Due to limited space, we show results on one random sample from only the B100 [15] and Urban100 [7] datasets. For each network, the following information is visualized: (i) individual outputs of each branch (P_0, \dots, P_n), (ii) the result formed after each branch ($I_0^{SR}, \dots, I_n^{SR}$), and (iii) the residuals i.e error maps after introducing each branch (R_1, \dots, R_{n+1}). It is easily visible that residual branches successfully learn high frequency information i.e. edges which contain most of the error in preceding predictions; incorporating such information at test time leads to reduced residuals after each branch.

¹<https://github.com/muneebaadil/sisr-irl>



(a) 108005.png from B100 [15]



(b) img043.png from Urban100 [7]

Figure 5: Qualitative Results of adding IRL framework to the existing state of the art methods.

5. Conclusions and Future Work

In this work, we argued that processing wholly on LR space – as recent state of the arts do – is sub-optimal. Furthermore, since recent methods take as input LR image, it is not possible, as a consequence, to learn residuals in image space. We address aforementioned issues by introducing residual branches which take as input the higher dimensional feature maps of master branch *i.e.* arbitrary pre-trained SR network, and predicts its residuals. We showed

empirically that doing so consistently enhances the performance of existing state of the art networks. Furthermore, we showed that L_2 loss on residual branches outperforms L_1 loss because residual branches explicitly model high frequency information as opposed to master branch which directly models HR image as a whole.

We show through extensive experiments on benchmark datasets that adding residual branches to existing state of the arts consistently outperform their original performance.

That being said, training residual branches require (i) no extra memory relative to master branch overhead because only one branch is trained at a time, and (ii) a mere 20% training time addition because only residuals are to be learnt.

Lastly, it is worth emphasizing that the network architectures used in residual branches are identical to the ones used in master branch due to simplicity. However, it is possible that optimizing network architecture in residual branches leads to superior performance because the nature of the learning goal in master branch is different than in residual branches. Thus, cross validating the network architecture for residual branches can prove to be promising direction.

6. Acknowledgements

We would like to acknowledge the computational grant from Higher Education Commission (HEC) of Pakistan.

References

- [1] E. Agustsson and R. Timofte. Ntire 2017 challenge on single image super-resolution: Dataset and study. In *The IEEE Conference on Computer Vision and Pattern Recognition (CVPR) Workshops*, July 2017.
- [2] M. Bevilacqua, A. Roumy, C. Guillemot, and M. L. Alberi-Morel. Low-complexity single-image super-resolution based on nonnegative neighbor embedding. 2012.
- [3] C. Dong, C. C. Loy, K. He, and X. Tang. Image super-resolution using deep convolutional networks. *IEEE transactions on pattern analysis and machine intelligence*, 38(2):295–307, 2016.
- [4] D. Glasner, S. Bagon, and M. Irani. Super-resolution from a single image. *2009 IEEE 12th International Conference on Computer Vision*, pages 349–356, 2009.
- [5] K. He, X. Zhang, S. Ren, and J. Sun. Deep residual learning for image recognition. In *Proceedings of the IEEE Conference on Computer Vision and Pattern Recognition*, pages 770–778, 2016.
- [6] G. Huang, Z. Liu, L. van der Maaten, and K. Q. Weinberger. Densely connected convolutional networks. *2017 IEEE Conference on Computer Vision and Pattern Recognition (CVPR)*, pages 2261–2269, 2017.
- [7] J.-B. Huang, A. Singh, and N. Ahuja. Single image super-resolution from transformed self-exemplars. In *Proceedings of the IEEE Conference on Computer Vision and Pattern Recognition*, pages 5197–5206, 2015.
- [8] J. Johnson, A. Alahi, and L. Fei-Fei. Perceptual losses for real-time style transfer and super-resolution. In *ECCV*, 2016.
- [9] J. Kim, J. Kwon Lee, and K. Mu Lee. Accurate image super-resolution using very deep convolutional networks. In *Proceedings of the IEEE Conference on Computer Vision and Pattern Recognition*, pages 1646–1654, 2016.
- [10] J. Kim, J. Kwon Lee, and K. Mu Lee. Deeply-recursive convolutional network for image super-resolution. In *Proceedings of the IEEE conference on computer vision and pattern recognition*, pages 1637–1645, 2016.
- [11] D. P. Kingma and J. Ba. Adam: A method for stochastic optimization. *CoRR*, abs/1412.6980, 2014.
- [12] W.-S. Lai, J.-B. Huang, N. Ahuja, and M.-H. Yang. Deep laplacian pyramid networks for fast and accurate super-resolution. In *IEEE Conference on Computer Vision and Pattern Recognition*, volume 2, page 5, 2017.
- [13] C. Ledig, L. Theis, F. Huszar, J. Caballero, A. Cunningham, A. Acosta, A. P. Aitken, A. Tejani, J. Totz, Z. Wang, and W. Shi. Photo-realistic single image super-resolution using a generative adversarial network. *2017 IEEE Conference on Computer Vision and Pattern Recognition (CVPR)*, pages 105–114, 2017.
- [14] B. Lim, S. Son, H. Kim, S. Nah, and K. M. Lee. Enhanced deep residual networks for single image super-resolution. In *The IEEE Conference on Computer Vision and Pattern Recognition (CVPR) Workshops*, July 2017.
- [15] D. Martin, C. Fowlkes, D. Tal, and J. Malik. A database of human segmented natural images and its application to evaluating segmentation algorithms and measuring ecological statistics. In *Computer Vision, 2001. ICCV 2001. Proceedings. Eighth IEEE International Conference on*, volume 2, pages 416–423. IEEE, 2001.
- [16] W. Shi, J. Caballero, F. Huszar, J. Totz, A. P. Aitken, R. Bishop, D. Rueckert, and Z. Wang. Real-time single image and video super-resolution using an efficient sub-pixel convolutional neural network. *2016 IEEE Conference on Computer Vision and Pattern Recognition (CVPR)*, pages 1874–1883, 2016.
- [17] K. Simonyan and A. Zisserman. Very deep convolutional networks for large-scale image recognition. *arXiv preprint arXiv:1409.1556*, 2014.
- [18] Y. Tai, J. Yang, and X. Liu. Image super-resolution via deep recursive residual network. In *Proceedings of the IEEE Conference on Computer Vision and Pattern Recognition*, 2017.
- [19] Y. Tai, J. Yang, X. Liu, and C. Xu. Memnet: A persistent memory network for image restoration. In *Proceedings of International Conference on Computer Vision*, 2017.
- [20] R. Timofte, R. Rothe, and L. V. Gool. Seven ways to improve example-based single image super resolution. *2016 IEEE Conference on Computer Vision and Pattern Recognition (CVPR)*, pages 1865–1873, 2016.
- [21] R. Timofte, V. D. Smet, and L. V. Gool. A+: Adjusted anchored neighborhood regression for fast super-resolution. In *ACCV*, 2014.
- [22] T. Tong, G. Li, X. Liu, and Q. Gao. Image super-resolution using dense skip connections. *2017 IEEE International Conference on Computer Vision (ICCV)*, pages 4809–4817, 2017.
- [23] Z. Wang and A. C. Bovik. Mean squared error: Love it or leave it? a new look at signal fidelity measures. *IEEE Signal Processing Magazine*, 26:98–117, 2009.
- [24] Z. Wang, A. C. Bovik, H. R. Sheikh, and E. P. Simoncelli. Image quality assessment: from error visibility to structural similarity. *IEEE Transactions on Image Processing*, 13:600–612, 2004.
- [25] J. Yang, Z. Wang, Z. L. Lin, S. Cohen, and T. S. Huang. Coupled dictionary training for image super-resolution. *IEEE Transactions on Image Processing*, 21:3467–3478, 2012.

- [26] J. Yang, J. Wright, T. S. Huang, and Y. Ma. Image super-resolution as sparse representation of raw image patches. *2008 IEEE Conference on Computer Vision and Pattern Recognition*, pages 1–8, 2008.
- [27] J. Yang, J. Wright, T. S. Huang, and Y. Ma. Image super-resolution via sparse representation. *IEEE Transactions on Image Processing*, 19:2861–2873, 2010.
- [28] R. Zeyde, M. Elad, and M. Protter. On single image scale-up using sparse-representations. In *International conference on curves and surfaces*, pages 711–730. Springer, 2010.
- [29] K. Zhang, X. Gao, D. Tao, and X. Li. Single image super-resolution with non-local means and steering kernel regression. *IEEE Transactions on Image Processing*, 21:4544–4556, 2012.
- [30] L. Zhang and X. Wu. An edge-guided image interpolation algorithm via directional filtering and data fusion. *IEEE Transactions on Image Processing*, 15:2226–2238, 2006.
- [31] Y. Zhang, Y. Tian, Y. Kong, B. Zhong, and Y. Fu. Residual dense network for image super-resolution. In *CVPR*, 2018.
- [32] H. Zhao, O. Gallo, I. Frosio, and J. Kautz. Loss functions for image restoration with neural networks. *IEEE Transactions on Computational Imaging*, 3:47–57, 2017.